ADVANCED MATERIALS
www.advmat.de

A Tandem Organic Solar Cell with PCE of 14.52% Employing Subcells with the Same Polymer Donor and Two Absorption Complementary Acceptors

Lingxian Meng, Yuan-Qiu-Qiang Yi, Xiangjian Wan, Yamin Zhang, Xin Ke, Bin Kan, Yanbo Wang, Ruoxi Xia, Hin-Lap Yip, Chenxi Li, and Yongsheng Chen**

The tandem structure is an efficient way to simultaneously tackle absorption and thermalization losses of the single junction solar cells. In this work, a high-performance tandem organic solar cell (OSC) using two subcells with the same donor poly[(2,6-(4,8-bis(5-(2-ethylhexyl)thiophen-2-yl)-benzo[1,2-b:4,5-b′]dithiophene))-*alt*-(5,5-(1′,3′-di-2-thienyl-5′,7′-bis(2-ethylhexyl)benzo[1′,2′-c:4′,5′-c′]dithiophene-4,8-dione))] (PBDB-T) and two acceptors, F-M and 2,9-bis(2-methylene-(3(1,1-dicyanomethylene)benz[f]indanone))7,12-dihydro-(4,4,10,10-tetrakis(4-hexylphenyl)-5,11-diocthylthieno[3′,2′:4,5]cyclopenta[1,2-b]thieno[2″,3″:3′,4′]cyclopenta[1′,2′:4,5]thieno[2,3-f][1]benzothiophene (NNBDT), with complementary absorptions is demonstrated. The two subcells show high V_{oc} with value of 0.99 V for the front cell and 0.86 V for the rear cell, which is the prerequisite for obtaining high V_{oc} of their series-connected tandem device. Although there is much absorption overlap for the subcells, a decent J_{sc} of the tandem cell is still obtained owing to the complementary absorption of the two acceptors in a wide range. With systematic device optimizations, a best power conversion efficiency of 14.52% is achieved for the tandem device, with a high V_{oc} of 1.82 V, a notable FF of 74.7%, and a decent J_{sc} of 10.68 mA cm^{-2}. This work demonstrates a promising strategy of fabricating high-efficiency tandem OSCs through elaborate selection of the active layer materials in each subcell and tradeoff of the V_{oc} and J_{sc} of the tandem cells.

Organic solar cells (OSCs) have made great progress in the past decade mainly thanks to the rapid development and evolution of donor and acceptor materials along with device engineering.[1–8] Power conversion efficiencies (PCEs) of single bulk heterojunction (BHJ)-based OSCs with fullerene derivatives acceptors have reached over 11%,[9,10] and nonfullerene-acceptor-based OSC devices even have achieved PCEs over 14%.[11–14] However, the current photovoltaics performance of OSCs is still in demand to be further improved when compared with other photovoltaic technologies.[15–18] Single junction OSCs normally suffer from the limited sunlight absorptions and the thermalization loss of photon energy. The tandem concept with stacking two or more subcells in series or parallel connection could address the above issues.[19–25] For the widely studied series-connected tandem cells, the overall open circuit voltage (V_{oc}) of the tandem cell is the sum of the V_{oc} values of the subcells if no potential losses in the interconnection layer.[24,25] The current density (J_{sc}) is generally limited by the subcell with the smallest one.[20,25] In order to pursue high PCEs for the series-connected tandem cell, there are several important factors should be considered synergistically. First, the subcells should have complementary absorptions and well balanced, and high J_{sc}. Second, the two subcells should have minimal energy loss to retain high V_{oc} and thus guarantee the whole high V_{oc} for the tandem devices. Third, the interconnection layer should attain efficient charge extraction and much reduced recombination.

In the past decade, great efforts have focused on searching for subcells with efficient light absorptions in a wide range with complementary absorption spectra and minimal absorption overlap.[26–32] For the fullerene derivatives based devices, it is expected to obtain a well-balanced J_{sc} through appropriate selection of donor materials with different bandgaps since fullerene derivatives have limited absorptions and their contribution on J_{sc} is much smaller than that of the donor materials. To date, PCEs ≈13% have been achieved for the fullenere-based tandem OSCs.[33] The reasons exist in two aspects for the likely ceiling efficiencies of fullerene derivatives based tandem OSCs.[28] The first one is the lack of suitable donor materials, especially narrow bandgap donors utilized for rear cells to achieve the high and balanced J_{sc} for tandem cells. The second one is the general large energy loss of the fullerene

L. Meng, Y.-Q.-Q. Yi, Dr. X. Wan, Y. Zhang, X. Ke, B. Kan, Y. Wang, Prof. C. Li, Prof. Y. Chen
The Key Laboratory of Functional Polymer Materials
State Key Laboratory and Institute of Elemento-Organic Chemistry
Centre of Nanoscale Science and Technology
College of Chemistry
Nankai University
Tianjin 300071, China
E-mail: xjwan@nankai.edu.cn; yschen99@nankai.edu.cn
R. Xia, Prof. H.-L. Yip
State Key Laboratory of Luminescent Materials and Devices
South China University of Technology
Guangzhou 510640, China
The ORCID identification number(s) for the author(s) of this article can be found under https://doi.org/10.1002/adma.201804723.

DOI: 10.1002/adma.201804723

acceptors based subcells and thus low V_{oc} of the final tandem devices. In contrast, for the nonfullerene-acceptor-based OSCs, both the donor and acceptor play the same vital roles in the light absorptions and make contributions to the J_{sc} equally, which would give more opportunities of achieving high J_{sc} for the tandem device. Besides, nonfullerene-based devices generally have smaller energy loss and thus higher V_{oc} than the devices based on fullerene derivatives.[4,6,7] Indeed, more and more attentions have been paid to the nonfullerene-acceptor-based tandem OSCs and promising results have been achieved in recent years. For example, Yan and co-workers recently reported a double-junction tandem solar cell with identical subcells based on P3TEA:SF-PDI$_2$, exhibiting a PCE of 10.8% with a high V_{oc} over 2.1 V.[34] A tandem OSC with a certified PCE 14.0% was reported by Hou and co-workers through optimizing the active layers absorptions of two nonfullerene-acceptor-based subcells.[35] Recently, Forrest and co-workers demonstrated a tandem cell with a 14.3% PCE using an evaporated small-molecule system as front cell and an infrared absorbing nonfullerene-based rear cell. After deposition of an antireflection coating on the glass substrate, an improved PCE of 15% was obtained.[36] Just recently, we have reported a tandem cell with a remarkable 17.3% PCE using two nonfullerene-acceptor (NFA) subcells with well-matched absorptions in the range of 300–1050 nm.[37]

As aforementioned discussions, the study focus of tandem OSCs is to design subcells active layers with complementary absorptions. However, with carefully check on the reported tandem OSCs, it is found that there are actually no subcells systems to fully meet the requirements for ideal tandem OSCs, especially from the perspective of completely complementary absorption, which could be observed from the external quantum efficiency (EQE) curves of those tandem OSCs.[7,28] It raises a question: could high-performance tandem OSCs be obtained without excessively consideration of the complementary absorptions of the subcells. Herein, we wish to report a tandem OSC employing two subcells with the same donor PBDB-T and two acceptors F-M and NNBDT with complementary absorptions. In our case, a high V_{oc} of the tandem cell was realized ascribed to the high V_{oc} of the two subcells owing to the deep the highest occupied molecular orbital (HOMO) of polymer donor PBDB-T. Meanwhile, the decent J_{sc} was obtained owing to the complementary absorptions of the two acceptors. With systematic devices optimizations, a PCE of 14.52% was achieved with a high V_{oc} of 1.82 V, a notable fill factor (FF) of 74.7%, and a decent J_{sc} of 10.68 mA cm^{-2}. This work demonstrated a promising strategy to fabricate high-efficiency tandem OSCs through careful selection of the subcells materials and tradeoff of the V_{oc} and J_{sc} of the tandem cells.

Figure 1a shows the chemical structures of the two acceptors F-M, NNBDT, and polymer donor PBDB-T. The two acceptors have recently been reported by our group.[38,39] PBDB-T was chosen as donor material since it could give high-performance devices with high V_{oc} owing to its deep HOMO. The absorption spectra of F-M, NNBDT, and PBDB-T films are shown in Figure 1b. The F-M film exhibits a maximum absorption peak (λ_{max}) at 687 nm. The NNBDT film shows absorption edge up to 900 nm with λ_{max} of 782 nm. The polymer PBDB-T gives absorption in the range 400–700 nm with λ_{max} at 628 nm. Clearly, the two small-molecule acceptors and the polymer donor show well complementary absorptions in a wide range of the solar spectrum from 300 to 900 nm.

Before the tandem device fabrication, the single junction OSC devices PBDB-T:F-M and PBDB-T:NNBDT with an inverted structure were fabricated and fully optimized. The device based on PBDB-T:F-M showed a PCE over 10%, with a high V_{oc} of

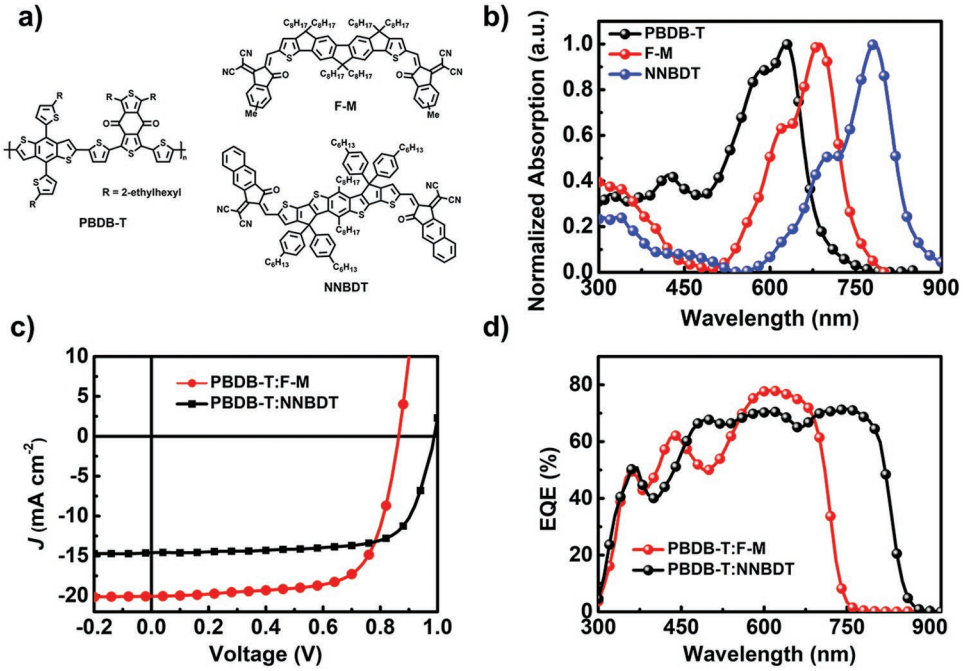

Figure 1. a) Chemical structure of acceptors F-M, NNBDT, and polymer donor PBDB-T used in the tandem OSCs. b) The absorptions of F-M, NNBDT, and polymer donor PBDB-T on solid films. c) *J*–*V* and d) EQE curves for the optimized devices of PBDB-T:F-M and PBDB-T:NNBDT with an architecture of ITO/ZnO/PFN-Br/active layer/MoO_x/Ag.

Table 1. The photovoltaic performance of the single-junction devices based on PBDB-T:F-M and PBDB-T:NNBDT.

Active layer	V_{oc} [V]	J_{sc} [mA cm^{-2}]	FF [%]	PCE [%][a)]
PBDB-T:F-M[b)]	0.99 ± 0.01 (0.99)	14.32 ± 0.23 (14.60)	71.6 ± 1.6 (72.7)	10.18 ± 0.13 (10.49)
PBDB-T:NNBDT[b)]	0.86 ± 0.01 (0.86)	20.06± 0.11 (20.07)	68.6 ± 0.6 (69.7)	11.87 ± 0.11 (12.03)

[a)]The average values are obtained from over ten independent cells, and the optimal results are provided in parentheses; [b)]The device architecture is ITO/ZnO/PFN-Br/active layer/MoO_x/Ag. The spin speed for PBDB-T:F-M is 3000 rpm and for PBDB-T:NNBDT is 1300 rpm.

≈0.99 V and a J_{sc} over 14 mA cm^{-2}. PBDB-T:NNBDT-based device gave a desirable V_{oc} (≈0.86 V) attributed to the deep HOMO level of PBDB-T. Note that the high J_{sc} of 20 mA cm^{-2} was achieved mainly owing to the broad absorption of PBDB-T:NNBDT, especially in the near-infrared region. The detailed photovoltaic parameters of the above two devices are summarized in **Table 1**. EQE curves of two optimized single-junction devices are shown in Figure 1d. Since the same donor polymer was used, there exists much EQE curve overlap for the two single junction devices in the range of 300–750 nm. However, the PBDB-T:NNBDT-based device exhibited excellent EQE values in the range of 750–900 nm where the PBDB-T:F-M device has no EQE response. For the state-of-the-art single junction OSCs, most of the ideal photoactive layer thickness is limited to around 100 nm owing to the low carrier mobilities, which limits overall absorption only between 60% and 80%.[40] It implies that in a tandem device, the rear cell could utilize the light in the overlap range passing through the front cell. As such in our case, a much decent J_{sc} could still be expected in the tandem cells.

As shown in **Figure 2**a, the inverted tandem devices were fabricated using all solution processing, except for the silver metal electrode. A fully solution-processed interconnection layer consisting of a modified poly(3,4-ethylenedioxythiopene):poly-(styrenesulfonate) (PEDOT:PSS) and a ZnO nanoparticles layer was used. Note that the optical modeling based on the transfer matrix (TM) method was conducted to provide guidance for the optimal thicknesses of the subcells prior to the tandem device fabrication.[41] As shown in Figure 2b, the simulated J_{sc} reaches an optimum value of 12.71 mA cm^{-2} when the thicknesses of the front and rear layers are 115 and 100 nm, respectively. Then, the tandem devices were optimized under the guidance of the above optical simulation results. A best PCE of 14.52% is achieved, with a V_{oc} of 1.82 V, a FF of 74.7%, and a J_{sc} of 10.68 mA cm^{-2} (Figure 2c) when the thicknesses of the front and rear cell are 105 and 110 nm, respectively. The detailed optimized parameters are summarized in **Table 2**. As shown in Table 2, the tandem devices all give high decent performance with PCEs above 12% with high V_{oc} of 1.80 V and notable FF over 70%. The V_{oc} of ≈1.82 V is approximately equal to the sum of individual V_{oc} of the subcells. The slightly low V_{oc} loss might be induced by interconnection layer between the two subcells, which is widely reported in literatures.[24,25,42]

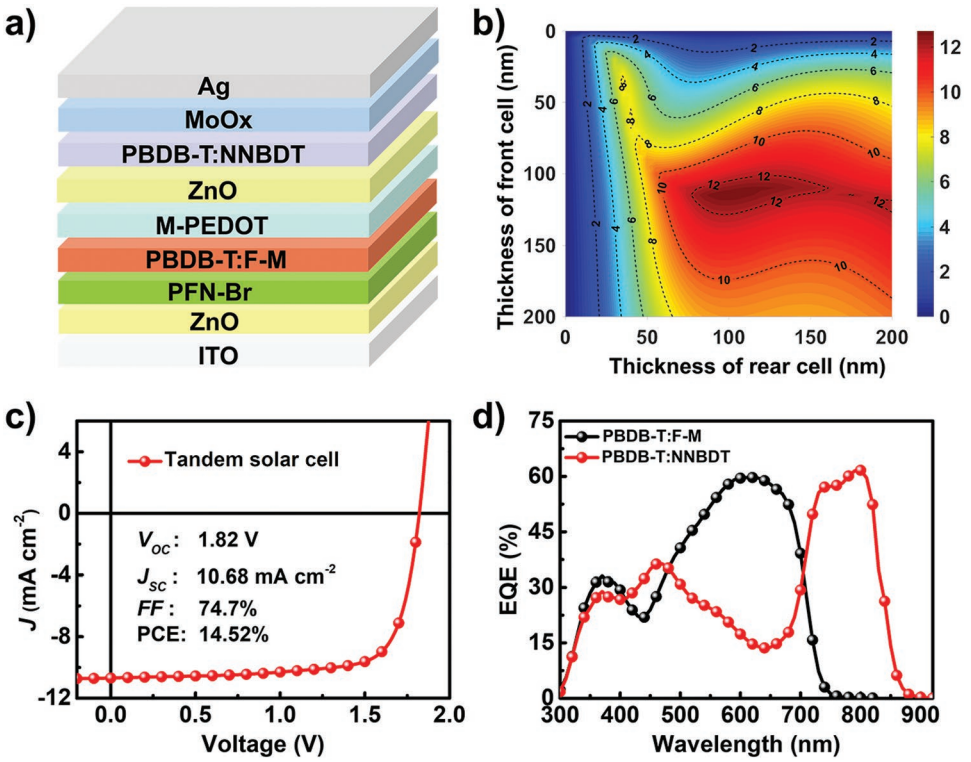

Figure 2. a) Device architecture of the tandem OSC. b) Simulated J_{sc} generated in tandem OSC as a function of thickness of the front and rear cells. c) Optimal *J–V* curve of the tandem OSC under the illumination of AM 1.5G (100 mW cm^{-2}). d) EQE curves of the front and rear cells.

Table 2. Tandem device performances with different thicknesses of the subcells.

Thickness [nm]		V_{oc} [V]	J_{sc} [mA cm^{-2}]	FF [%]	PCE [%][a)]
Front subcell	Rear subcell				
90	110	1.81 ± 0.01 (1.82)	10.15 ± 0.23(10.20)	72.7 ± 0.6 (73.0)	13.31 ± 0.03(13.54)
105	110	1.81 ± 0.01 (1.82)	10.59 ± 0.12(10.68)	73.2 ± 0.9 (74.7)	14.03 ± 0.25 (14.52)[b)]
125	110	1.81 ± 0.01 (1.81)	9.52 ± 0.22 (9.83)	71.2 ± 0.8 (70.0)	12.25 ± 0.29(12.42)
105	95	1.81 ± 0.01 (1.80)	10.38 ± 0.13(10.41)	72.1 ± 0.6 (73.0)	13.55 ± 0.03(13.68)
105	135	1.81 ± 0.01 (1.81)	10.70 ± 0.18(10.94)	70.6 ± 0.5 (69.9)	13.67 ± 0.29(13.84)

[a)]Statistical and optimal results are listed outside of parentheses and in parentheses, respectively, and the average parameters were calculated from more than 20 independent cells; [b)]The PCE of optimized devices were also measured using mask, and the results are similar as shown in detail in Table S1 in the Supporting Information.

The EQE of the optimized tandem device was measured and shown in Figure 2d. The front cell shows photoresponse in the range of 300–720 nm with maximum response of ≈60% at 620 nm. The rear cell exhibits strong EQE response from ≈700 to 850 nm with a maximum value 61%. Besides, the rear cell shows 14–36% EQE height in the range of 350–700 nm. It indicates the front cell could not completely absorb the light in its absorption range, some of which passed to the rear cell and were absorbed and thus contributed to the current of the rear cell. The J_{sc} values obtained by integration of the EQE curves are 9.94 mA cm^{-2} for the front subcell and 10.00 mA cm^{-2} for the rear subcell, which are consistent with the J_{sc} of the tandem device obtained from current–density (J–V) measurement under AM 1.5G illumination and indicated high balanced current generation in each subcell.

Besides, the light intensity dependence of our tandem cell performance was measured under different light intensity (**Figure 3**). The detailed photovoltaic parameters under different light intensity are given in Table S2 in the Supporting Information. The PCEs of the tandem device keep over 14% when the light intensity varies from 5 to 100 mW cm^{-2}, and a PCE of 15.15% was achieved at the light intensity of 14.67 mW cm^{-2}, which indicates that the tandem device could work efficiently under varied light intensities. In addition, a linear relationship between the light intensity and short-circuit current density was observed (Figure 3b), indicating the space charge effects can be neglected in the tandem device and the interconnection layer.[2] Moreover, the stability of tandem solar cell was briefly tested. As shown in Figure S1 in the Supporting Information, the tandem device exhibited good stability with a PCE of 13.51% (93% of its initial PCE) after 17 d storage in the glove box.

The wavelength-dependent energy conversion curves for the two subcells and the tandem cells are depicted in Figure 3c. In contrast to the subcells, the tandem device clearly achieved an improved photovoltaic performance, which is attributed to both the complementary and overlapped absorptions of the two subcells. Considering that different materials with different band structure, Eloss, FF would impact the PCEs significantly, we have done a semiexpirical modeling for the possible PCEs. As depicted in Figure S2 in the Supporting Information, once those parameters could be improved and enhanced, significantly elevated PCEs would be expected in the near future for the tandem cell with the same donor material. Presently, there are actually no subcells systems to fully meet the requirements for ideal tandem OSCs such as completely complementary absorption, low energy loss, and etc.[7,28] Our case together with the calculation results shows that the strategy of utilization of the same donor material and tradeoff of the V_{oc} and J_{sc}, without excessively pursuing for the subcells with well complementary absorptions, is an alternative and effective way to achieve high-performance tandem OSCs.

In summary, we have demonstrated a highly efficient tandem OSC using two subcells with the same donor PBDB-T and two acceptors F-M and NNBDT with complementary absorptions. The standpoint for the design is to obtain the balanced V_{oc} and J_{sc} and then to get a high efficiency for the tandem OSC. In our case, the optimized PCE of 14.52% has been achieved, with a high V_{oc} of 1.82 V, a notable FF of 74.7%, and a J_{sc} of 10.68 mA cm^{-2}. This work has demonstrated a promising strategy for fabricating

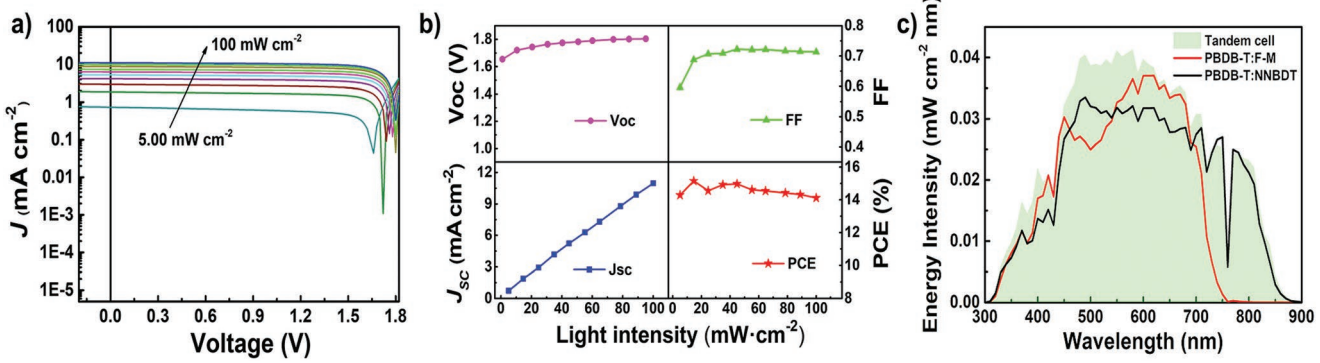

Figure 3. a) J–V curve and b) variation of photovoltaic parameters of the tandem devices under different light intensity from 5 to 100 mW cm^{-2}. c) Wavelength-dependent energy density for the subcells and tandem cells (using the method in ref. [43]).

high-efficiency tandem OSCs through subtle tradeoff of the V_{oc} and J_{sc}, especially at the present time when there are few matched subcells active materials with real complementary absorptions to fully meet the requirements of ideal tandem cells.

Experimental Section

Materials: PBDB-T was purchased from Solarmer Materials Inc. F-M and NNBDT were synthesized following the previous reports.[38,39] All chemicals and solvents were reagent grades and purchased from Sigma-Aldrich and Alfa Aesar, respectively.

Single Cell Device Fabrication: The device structure was indium tin oxide (ITO)/ZnO/PFN-Br/active layer/MoO_x/Ag. A layer of ZnO (≈30 nm) was deposited by spin coating a ZnO precursor on top of precleaned ITO substrates and annealed at 200 °C for 1 h in air. Subsequently, a thin layer of PFN-Br was spin coated on the ZnO layer. Then the blend solution of PBDB-T:F-M (1: 1 w/w, 11 mg mL^{-1}, from CB with 0.2% DIO) was spin coated at 3000 rpm for 40 s or PBDB-T:NNBDT (1:0.8 w/w, 7 mg mL^{-1}, from CF with 0.5% DIO) was spin coated at 1300 rpm for 20 s to form the active layer. For PBDB-T:NNBDT devices, annealed at 120 °C for 10 min. A MoO_x layer (6 nm) and an Ag layer (70 nm) were then deposited on the active layer by vacuum evaporation under 2×10^{-4} Pa.

Tandem Cell Device Fabrication: The tandem devices were fabricated with an architecture of ITO/ZnO/PFN-Br/PBDB-T:F-M/M-PEDOT/ZnO/PBDB-T:NNBDT/MoO_x/Ag. The PBDB-T:F-M active layers were fabricated via the same process as the single cells with different thicknesses. Subsequently, the M-PEDOT (Clevious P VP Al 4083 diluted with equal volume of isopropyl alcohol and 0.3 wt% of Zonyl FSN) (≈50 nm) was spin coated on top of the active layer of the front subcell, followed by annealing at 120 °C for 10 min, and then ZnO nanoparticles layer (≈15 nm) was spin coated and annealed at 120 °C for 10 min. Then, the PBDB-T:NNBDT active layers were fabricated with the same process as the single cells with different thicknesses, followed by annealing at 120 °C for 10 min. A MoO_x layer (≈6 nm) and an Ag layer (≈70 nm) were then deposited on the active layer by vacuum evaporation under 2×10^{-4} Pa. The effective areas of cells were ≈4 mm^2 defined by shallow masks.

Device Characterization: The *J–V* curves of fabricated devices were obtained by a Keithley 2400 source-measure unit. The photocurrent was measured under AM 1.5G illumination at 100 mW cm^{-2} irradiation using a Enli SS-F5-3A solar simulator, calibrated with a standard Si solar cell (made by Enli Technology Co., Ltd., Taiwan, and calibrated report can be traced to NREL). The thickness of the active layers in the photovoltaic devices was measured under a Veeco Dektak 150 profilometer. The EQE spectrum was measured using a QE-R Solar Cell Spectral Response Measurement System (Enli Technology Co., Ltd., Taiwan). To measure the rear and front cell, light bias obtained by 550 nm low-pass optical filters and 700 nm high-pass were selected to excite (saturate) the front and rear cells, respectively. Electrical biases of 0.8 and 0.9 V were applied on the tandem OSCs to measure the front and rear subcells, respectively. The mismatch factor M values of both subcells under the solar simulator were calculated according to ref. [44] and the values were around 1 (1.008 for the front cell and 1.032 for the rear cell).

In order to investigate the dependence of the *J–V* measurements under different light intensities, a neutral density sieve was used to modulate the light intensity, and a standard Si solar cell was used to calibrate the light intensity.

The optical model was preformed based on the TM formalism model. The refractive index (*n*) and extinction coefficient (*k*) spectra of each layer in the devices were measured using a J.A. WOOLAM Co. V-VASE ellipsometer (VB-400 Control Module).

Supporting Information

Supporting Information is available from the Wiley Online Library or from the author.

Acknowledgements

L.M. and Y.-Q.-Q.Y. contributed equally to this work. The authors gratefully acknowledge the financial support from MoST (2016YFA0200200), NSFC (51773095, 91633301) of China, Tianjin city (17JCJQJC44500, 17JCZDJC31100), and 111 Project (B12015).

Conflict of Interest

The authors declare no conflict of interest.

Keywords

nonfullerene acceptors, organic solar cells, tandem devices

Received: July 23, 2018
Revised: January 19, 2019
Published online:

[1] M. C. Scharber, N. S. Sariciftci, *Prog. Polym. Sci.* **2013**, *38*, 1929.
[2] J. Y. Kim, K. Lee, N. E. Coates, D. Moses, T. Q. Nguyen, M. Dante, A. J. Heeger, *Science* **2007**, *317*, 222.
[3] H. Feng, M. Li, W. Ni, B. Kan, Y. Wang, Y. Zhang, H. Zhang, X. Wan, Y. Chen, *Sci. China Chem.* **2017**, *60*, 552.
[4] J. Hou, O. Inganas, R. H. Friend, F. Gao, *Nat. Mater.* **2018**, *17*, 119.
[5] Z. He, B. Xiao, F. Liu, H. Wu, Y. Yang, S. Xiao, C. Wang, T. P. Russell, Y. Cao, *Nat. Photonics* **2015**, *9*, 174.
[6] G. Zhang, J. Zhao, P. C. Y. Chow, K. Jiang, J. Zhang, Z. Zhu, J. Zhang, F. Huang, H. Yan, *Chem. Rev.* **2018**, *118*, 3447.
[7] P. Cheng, G. Li, X. Zhan, Y. Yang, *Nat. Photonics* **2018**, *12*, 131.
[8] V. Vohra, K. Kawashima, T. Kakara, T. Koganezawa, I. Osaka, K. Takimiya, H. Murata, *Nat. Photonics* **2015**, *9*, 403.
[9] J. Wan, X. Xu, G. Zhang, Y. Li, K. Feng, Q. Peng, *Energy Environ. Sci.* **2017**, *10*, 1739.
[10] D. Deng, Y. Zhang, J. Zhang, Z. Wang, L. Zhu, J. Fang, B. Xia, Z. Wang, K. Lu, W. Ma, Z. Wei, *Nat. Commun.* **2016**, *7*, 13740.
[11] S. Zhang, Y. Qin, J. Zhu, J. Hou, *Adv. Mater.* **2018**, *30*, 1800868.
[12] Z. Xiao, X. Jia, L. Ding, *Sci. Bull.* **2017**, *62*, 1562.
[13] S. Li, L. Ye, W. Zhao, H. Yan, B. Yang, D. Liu, W. Li, H. Ade, J. Hou, *J. Am. Chem. Soc.* **2018**, *140*, 7159.
[14] Z. Zheng, Q. Hu, S. Zhang, D. Zhang, J. Wang, S. Xie, R. Wang, Y. Qin, W. Li, L. Hong, N. Liang, F. Liu, Y. Zhang, Z. Wei, Z. Tang, T. P. Russell, J. Hou, H. Zhou, *Adv. Mater.* **2018**, *30*, 1801801.
[15] A. Polman, M. Knight, E. C. Garnett, B. Ehrler, W. C. Sinke, *Science* **2016**, *352*, aad4424.
[16] W. S. Yang, J. H. Noh, N. J. Jeon, Y. C. Kim, S. Ryu, J. Seo, S. I. Seok, *Science* **2015**, *348*, 1234.
[17] K. Yoshikawa, H. Kawasaki, W. Yoshida, T. Irie, K. Konishi, K. Nakano, T. Uto, D. Adachi, M. Kanematsu, H. Uzu, K. Yamamoto, *Nat. Energy* **2017**, *2*, 17032.
[18] S. Essig, C. Allebe, T. Remo, J. F. Geisz, M. A. Steiner, K. Horowitz, L. Barraud, J. S. Ward, M. Schnabel, A. Descoeudres, D. L. Young, M. Woodhouse, M. Despeisse, C. Ballif, A. Tamboli, *Nat. Energy* **2017**, *2*, 17144.
[19] A. Hadipour, B. de Boer, P. W. M. Blom, *Adv. Funct. Mater.* **2008**, *18*, 169.
[20] G. Dennler, M. C. Scharber, T. Ameri, P. Denk, K. Forberich, C. Waldauf, C. J. Brabec, *Adv. Mater.* **2008**, *20*, 579.
[21] L. Yang, H. Zhou, S. C. Price, W. You, *J. Am. Chem. Soc.* **2012**, *134*, 5432.

[22] S. Lu, X. Guan, X. Li, W. E. I. Sha, F. Xie, H. Liu, J. Wang, F. Huang, W. C. H. Choy, *Adv. Energy Mater.* **2015**, *5*, 1500631.
[23] O. Adebanjo, P. P. Maharjan, P. Adhikary, M. Wang, S. Yang, Q. Qiao, *Energy Environ. Sci.* **2013**, *6*, 3150.
[24] S. Sista, Z. Hong, L.-M. Chen, Y. Yang, *Energy Environ. Sci.* **2011**, *4*, 1606.
[25] T. Ameri, N. Li, C. J. Brabec, *Energy Environ. Sci.* **2013**, *6*, 2390.
[26] Y. Cui, H. Yao, B. Gao, Y. Qin, S. Zhang, B. Yang, C. He, B. Xu, J. Hou, *J. Am. Chem. Soc.* **2017**, *139*, 7302.
[27] S. Song, K. Kranthiraja, J. Heo, T. Kim, B. Walker, S.-H. Jin, J. Y. Kim, *Adv. Energy Mater.* **2017**, *7*, 1700782.
[28] G. Li, W. Chang, Y. Yang, *Nat. Rev. Mater.* **2017**, *2*, 17043.
[29] W. Li, A. Furlan, K. H. Hendriks, M. M. Wienk, R. A. J. Janssen, *J. Am. Chem. Soc.* **2013**, *135*, 5529.
[30] J. You, L. Dou, K. Yoshimura, T. Kato, K. Ohya, T. Moriarty, K. Emery, C.-C. Chen, J. Gao, G. Li, Y. Yang, *Nat. Commun.* **2013**, *4*, 1446.
[31] F. Chen, J. Xu, Z. Liu, M. Chen, R. Xia, Y. Yang, T. K. Lau, Y. Zhang, X. Lu, H. L. Yip, A. K. Jen, H. Chen, C. Li, *Adv. Mater.* **2018**, *30*, 1803769.
[32] Y. Li, J. D. Lin, X. Liu, Y. Qu, F. P. Wu, F. Liu, Z. Q. Jiang, S. R. Forrest, *Adv. Mater.* **2018**, *30*, 1804416.
[33] M. Li, K. Gao, X. Wan, Q. Zhang, B. Kan, R. Xia, F. Liu, X. Yang, H. Feng, W. Ni, Y. Wang, J. Peng, H. Zhang, Z. Liang, H.-L. Yip, X. Peng, Y. Cao, Y. Chen, *Nat. Photonics* **2017**, *11*, 85.
[34] S. Chen, G. Zhang, J. Liu, H. Yao, J. Zhang, T. Ma, Z. Li, H. Yan, *Adv. Mater.* **2017**, *29*, 1604231.
[35] Y. Cui, H. Yao, C. Yang, S. Zhang, J. Hou, *Acta Polym. Sin.* **2018**, *2*, 223.
[36] X. Che, Y. Li, Y. Qu, S. R. Forrest, *Nat. Energy* **2018**, *3*, 422.
[37] L. Meng, Y. Zhang, X. Wan, C. Li, X. Zhang, Y. Wang, X. Ke, Z. Xiao, L. Ding, R. Xia, H.-L. Yip, Y. Cao, Y. Chen, *Science* **2018**, *361*, 1094.
[38] B. Kan, Y. Yi, X. Wan, H. Feng, X. Ke, Y. Wang, C. Li, Y. Chen, *Adv. Energy Mater.* **2018**, *8*, 1800424.
[39] Y. Zhang, B. Kan, Y. Sun, Y. Wang, R. Xia, X. Ke, Y. Q. Yi, C. Li, H. L. Yip, X. Wan, Y. Cao, Y. Chen, *Adv. Mater.* **2018**, *30*, 1707508.
[40] J. You, C. C. Chen, Z. Hong, K. Yoshimura, K. Ohya, R. Xu, S. Ye, J. Gao, G. Li, Y. Yang, *Adv. Mater.* **2013**, *25*, 3973.
[41] G. F. Burkhard, E. T. Hoke, M. D. McGehee, *Adv. Mater.* **2010**, *22*, 3293.
[42] X. Du, O. Lytken, M. S. Killian, J. Cao, T. Stubhan, M. Turbiez, P. Schmuki, H.-P. Steinrück, L. Ding, R. H. Fink, N. Li, C. J. Brabec, *Adv. Energy Mater.* **2017**, *7*, 1601959.
[43] L. Zuo, X. Shi, S. B. Jo, Y. Liu, F. Lin, A. K. Jen, *Adv. Mater.* **2018**, *30*, 1706816.
[44] R. Timmreck, T. Meyer, J. Gilot, H. Seifert, T. Mueller, A. Furlan, M. M. Wienk, D. Wynands, J. Hohl-Ebinger, W. Warta, R. A. J. Janssen, M. Riede, K. Leo, *Nat. Photonics* **2015**, *9*, 478.